Investigating hydrological model versatility to simulate extreme flood events

Daniela Peredo, Maria-Helena Ramos, Vazken Andréassian, Ludovic Oudin

Investigating hydrological model versatility to simulate extreme flood events

Daniela Peredo, Maria-Helena Ramos, Vazken Andréassian & Ludovic Oudin

Published online: 21 Feb 2022.

Submit your article to this journal

Article views: 192

View related articles

View Crossmark data

IAHS AISH

Taylor & Francis
Taylor & Francis Group

Investigating hydrological model versatility to simulate extreme flood events

Daniela Peredo [ID][a,b], Maria-Helena Ramos [ID][b], Vazken Andréassian [ID][b] and Ludovic Oudin [ID][a]

aUMR Metis, Sorbonne Université, Paris, France; bUniversité Paris-Saclay, INRAE, UR HYCAR, Antony, France

ABSTRACT

We adapted a semi-distributed hydrological model (GRSD) to improve its versatility to simulate flood events occurring under different conditions, especially flash floods after dry summer periods in the Mediterranean region. The adaptation introduces a dependency on rainfall intensity in the production function. The evaluation over 2008–2018 in the Aude catchment (France) showed that the new model structure does not deteriorate long-term model simulations obtained from the original model. The adapted model performed better than or equal to the original model in terms of differences in the timing of peak discharges, regardless of the season of the year when the flood occurs. The most important improvement was observed in the simulation of the magnitude of the flood peaks during autumn floods. A visualization of model versatility allows the detection of the time steps when the new model tends to behave more similarly to or differently from the original model in terms of runoff production.

1 Introduction

1.1 High-impact floods in the Mediterranean region

Floods are natural hazards with large potential social and economic impacts (human losses, property and public infrastructure damages, disruption of industrial activities, etc.). River floods occur more or less abruptly, depending on the characteristics of the catchment and on how its response is triggered by meteorological forcings (Viglione and Rogger 2015). Widespread river floods usually develop over long time scales (several days) and generally occur in large catchments as a result of persistent precipitation (Stein *et al.* 2020) and high levels of soil saturation (Berghuijs *et al.* 2019). Flash floods are characterized by fast rise times of water levels (often less than 6–12 hours), occurring typically in steep and small or medium-sized catchments. They are usually the result of high intensity, convective rain falling over catchments with localized saturated soils (Garambois *et al.* 2014, Douinot *et al.* 2018) or infiltration excess in areas where the soil has a reduced infiltration capacity (Alaoui *et al.* 2018). Understanding the space–time variability of flood-generating processes is key for effective catchment modelling and flood forecasting (Viglione *et al.* 2010).

In the Mediterranean region, high-impact flood events are often the result of a combination of local climate, which is influenced by its proximity to the Mediterranean Sea, and the surrounding reliefs. The characteristics of rainfall generating damaging floods vary from (i) strongly convective, short-duration (less than one hour) rainfall with high intensities but limited total amounts to (ii) mesoscale convective systems producing long-lasting and stationary rainfall events over several hours, and (iii) sustained, heavy rainfall, embedded in large-scale perturbations lasting several days and often

covering large areas (Gaume *et al.* 2016, Llasat *et al.* 2016). Combined with different soil types and initial soil moisture conditions, rainfall events can generate varied catchment responses (see e.g. Delrieu *et al.* 2005, Borga *et al.* 2007, Le Lay and Saulnier 2007, Anquetin *et al.* 2010, Garambois *et al.* 2014, Faccini *et al.* 2016). Anticipating the response of Mediterranean catchments to heavy rainfall is crucial to organize actions and mitigate flood impacts. To support decision making, monitoring networks, real-time products and modelling tools need to be robustly designed and adapted to the conditions and particularities of high-impact flood events (Gourley *et al.* 2017).

1.2 Models to reproduce catchment dynamics and response to rainfall

There is a variety of rainfall-runoff modelling approaches in the literature. Conceptual models (mostly used by operational flood forecasting services) depend on parameters to be calibrated against observed discharges (Pagano *et al.* 2014). Physically based models are (in principle) able to run without calibration, but require a wealth of field data and higher computational time (Reed *et al.* 2004, Smith *et al.* 2012). Event-based models usually run faster than continuous models (in terms of computational time), but require significant efforts to estimate the catchment's initial conditions before a flood event (Vincendon *et al.* 2010, Roux *et al.* 2011, Nguyen and Bouvier 2019). Lumped models need to be calibrated at each catchment of interest, while semi-distributed or fully distributed (grid-based) models, combined with hydraulic propagation models, allow the simultaneous calibration of sub-catchments or modelling units inside a catchment.

Regardless of the modelling approach, hydrological models have a common goal of reproducing the catchment's dynamics and response to rainfall events. They often start by calculating the catchment production, i.e. the amount of runoff generated by the rainfall event, which will then be propagated to the catchment's outlet. Among the runoff mechanisms that guide the conceptualization of the complex interactions between storm properties, catchment characteristics and antecedent soil moisture conditions in hydrological models (Vivoni *et al.* 2007), the two more often considered are infiltration excess (Horton-type runoff; Horton 1945) and saturation excess (Dunne-type runoff; Dunne and Black 1970). The first is based on the assumption that all precipitation falling on the soil will infiltrate unless the surface soil layer is saturated or impervious (e.g. TOPKAPI model; Ciarapica and Todini 2002, Liu and Todini 2002). The second relies on saturation excess overland flow and on the variable source area concept, which refers to areas within a catchment where the soil becomes temporally saturated and runoff is generated (e.g. early versions of TOPMODEL; Beven and Kirkby 1979, Sivapalan *et al.* 1987).

Hydrological models may include one or both runoff mechanisms to calculate surface runoff generated by rainfall excess (or "net rainfall"). The description of the wetting and drying processes occurring in the upper layer(s) of the soil, which are responsible for the generation of surface runoff, can be formulated in different ways. The VIC model (Liang *et al.* 1994, Hamman *et al.* 2018), for instance, with a stand-alone land-surface scheme, relies on soil characteristics and an infiltration (or storage) capacity parameterization. The family of GR models (Perrin *et al.* 2003, Coron *et al.* 2017) uses a conceptual reservoir (called the "production reservoir"), with a calibrated parameter for the reservoir maximum storage capacity. The production reservoir receives a fraction of the net rainfall, which depends on both the net rainfall and the current state of the reservoir. Modelling choices to capture catchment dynamics are crucial to accurately simulate the hydrological response of soil surfaces to rainfall. Referring to TOPMODEL, for instance, Beven (1997) noted that including more dynamics in the contributing areas of the model may be important when modelling the response of a catchment after a long dry spell, when saturated zones may become localized and disconnected (see also Beven and Freer 2001).

1.3 Improving the versatility of rainfall-runoff models

The structure of hydrological models is based on a number of hypotheses and on the modeller's perceptions of the relevant processes to be considered in the rainfall-runoff transformation (Wagener *et al.* 2001). Perrin *et al.* (2003) recommended paying special attention to the main source of uncertainty (or what the modeller perceives as the main source of uncertainty) in the modelling process and using existing model structures as a starting point for further structural modifications. Recently, Addor and Melsen (2019) discussed the fact that hydrologists tend to stick to the model they have experience with when selecting a model for a particular study or area. They suggest using modular modelling frameworks to improve model adequacy for different purposes.

Model adaptation aims to better represent a catchment response, improve model versatility and, ultimately, model performance when applied to different conditions and for different hydrological applications. It may concern model flexibility to simulate flows at different temporal resolutions with the same model structure (Ficchì *et al.* 2019) or model ability to better represent processes in space (Garavaglia *et al.* 2017), knowing that spatial and temporal scales are intrinsically linked in hydrological processes and interact when evaluating model performance (Melsen *et al.* 2016). The search for versatile modelling frameworks has also been investigated by using different models with different structures to generate ensemble predictions (Velázquez *et al.* 2011, Seiller *et al.* 2012) and flexible (or modular) modelling frameworks to isolate individual model hypotheses of catchment behaviour and enable different model conceptualizations as alternative flux parameterizations (Clark *et al.* 2011, 2015, Fenicia *et al.* 2011, 2014). Van Esse *et al.* (2013) show that despite its merits, the flexible approach faces difficulties related to the identification of optimal model structures and parameter sets, inconsistencies in model performance when there are large climatic differences between the model calibration and validation periods, and increased complexity for applications in operational modelling or real-time forecasting.

1.4 Study aim

This paper aims to investigate how explicitly accounting for rainfall intensity in the production function of a hydrological model can improve model versatility and contribute to an improved simulation of flash floods, especially in the case of events that take place at the beginning of the hydrological year in the Mediterranean area, after a long dry summer period. The semi-distributed GRSD model (Lobligeois *et al.* 2014) is adapted to simulate two key types of flood events observed in the Aude catchment (France): winter and spring floods occurring during or after wet periods, and autumn floods occurring after dry summer periods. While the production rate function of the original model seeks to fill the production store when its level is low, regardless of rainfall intensity, the proposed adaptation seeks to integrate additional concepts of runoff generation as described by Ferré and Warrick (2005). When soils have low infiltration capacity or when net rainfall is larger than the infiltration capacity, excess water will become runoff and will not be stored in the production store. In the following, Section 2 presents the data, study area and methods applied, including the hydrological model, its adaptation and the evaluation approach. Section 3 presents the model performance results and the analysis of model versatility. Discussion and conclusions are presented in Section 4.

2 Data and methods

2.1 The GRSD semi-distributed rainfall-runoff model

GRSD is a semi-distributed hydrological model from the GR family of models (Perrin *et al.* 2001), which runs at an hourly time step (Lobligeois *et al.* 2014). It evolved from a five-parameter lumped hydrological model (Le Moine *et al.* 2008)
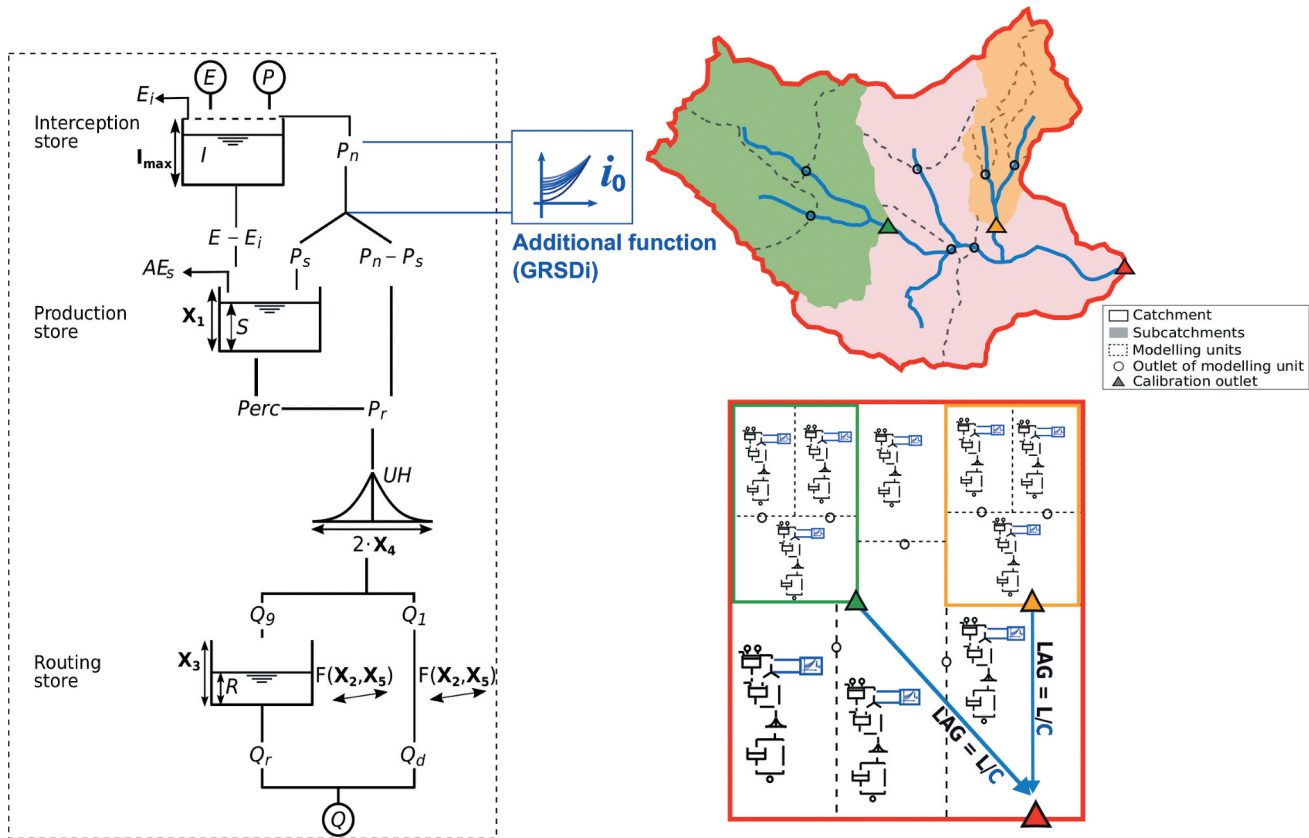
Figure 1. Representation of the hydrological modelling approach: GRSD model, based on parameters X_1 to X_5, in black, and GRSDi model, based on the additional parameter i_0, in blue (left), and scheme of the model semi-distribution within a catchment (right).

and a one-parameter linear lag propagation model (Bentura and Michel 1997) that propagates river flows downstream between lumped modelling units and from the subcatchments to the main outlet. The model structure is based on a sequence of production and routing functions and their five parameters (X_1 to X_5). The structure is represented in Fig. 1 (left) and the parameters are listed in Table 1. Precipitation (P) and potential evapotranspiration (E) are first processed through an interception store of fixed maximum capacity (I_{max}) of 2 [mm] (Ficchì *et al.* 2016), which evaporates water from the interception store (E_i) and allows us to obtain the net rainfall (P_n). Part of the net rainfall fills the production store (P_s) and part flows directly into the other components of the model for its routing to the outlet (P_r). These amounts of water (P_s and P_r) are determined by a function that depends on the level of the production store (S). This function is modified in this study to allow a higher amount of rainfall to bypass the production store when the

hourly rainfall intensity is high. The new model structure (GRSDi), with an additional parameter i_0 (Fig. 1 and Table 1), is detailed in Section 2.2.

After the production function, the sum of P_r and a percolation term (*Perc*; outgoing water from the production store) is routed by a symmetric unit hydrograph (*UH*). Its output is split into two: 90% of the water (Q_9) is sent to a non-linear routing store (R) and 10% (Q_1) reaches the outlet directly. An inter-catchment groundwater flow term (F) allows us to add (if positive) or remove (if negative) water from the routing store and the Q_1 component. Finally, the simulated streamflow (Q) is obtained by the sum of two flow components: the output from the routing reservoir, which represents a slow flow component (Q_r), and a component derived from Q_1, which represents a faster flow component (Q_d).

To take into account the spatial variability of the meteorological variables, the catchment is discretized into modelling units. Their delimitation considers all the gauged outlets (which define the gauged sub-catchments) and a predetermined modelling unit size, which is established by the user (de Lavenne *et al.* 2016, 2019). This target size for modelling units is used to create as many ungauged outlets as necessary within each gauged sub-catchment, while keeping the computational time low. Each modelling unit has its own meteorological input and runs the production-routing structure described above. Their outflows are propagated through a LAG function (Fig. 1, right), in which the average flow velocity (C [m s^{-1}]), a parameter to be calibrated (Table 1), is combined with the hydraulic distance between outlets L [m].

Table 1. Parameters of the semi-distributed hydrological models at the hourly time step: GRSD (1 to 6) and GRSDi (1 to 7).

No.	Model parameter	Description	Unit
1	X_1	Production store capacity	[mm]
2	X_2	Inter-catchment groundwater flow coefficient	[mm h^{-1}]
3	X_3	Routing store capacity	[mm]
4	X_4	Base time of the unit hydrograph	[h]
5	X_5	Threshold for the groundwater exchange	[-]
6	C	Average streamflow velocity	[m s^{-1}]
7	i_0	Characteristic rainfall intensity	[mm h^{-1}]

2.2 Accounting for the impact of rainfall intensity on the production rate

The model modification introduced aims to enhance the performance of the GRSD model when simulating flash floods, especially in the case of events that take place at the beginning of the hydrological year in the Mediterranean area, after a long dry period. A dependency on rainfall intensity is introduced in the production function of the model, when the production rate (i.e. the separation between P_s and P_r) is computed. To keep the model parsimonious, this is done by adding a single additional parameter to calibrate (i_0 [mm h^{-1}]; Fig. 1 and Table 1).

The production store in the GRSD model represents the evolution of the catchment moisture content at each time step. If there is still energy for evapotranspiration after the interception process over the time step, water will be withdrawn from the production store (AE_s, Fig. 1). The production store also receives part of the remaining net rainfall (P_s, Fig. 1), while the complementary part ($P_r = P_n - P_s$) adds to the percolation (Perc) of the production store to feed the subsequent functions of the model. The amount of water P_r is calculated as a fraction of the net rainfall (P_n). This fraction can be defined as a production rate (η, Equation (1)), which is obtained with a quadratic equation (Edijatno and Michel 1989):

$$\eta = \left[\frac{S}{X_1}\right]^2 \qquad (1)$$

where η is the production rate, which depends on the maximal capacity of the production store (X_1 [mm]) and on its level at each time step (S [mm], Fig. 1).

The reservoir level (S) increases progressively until the production store reaches its maximum value (X_1), and decreases under the effect of AE_s, until the production store is empty. The evolution of the production rate is shown in Fig. 2 (dashed line). The quadratic production rate function leads to low values of store outputs when the level of the production store is very low. Although this behaviour corresponds to the usual behaviour of natural catchments during extended dry periods, it may cause underestimation when simulating floods that occur after intense rainfall, when the catchment reacts even if the initial soil moisture content is low. This process is known as infiltration excess overland flow (Ferré and Warrick 2005). In order to simulate high flows with a higher production rate from rainfall even when the level of the production store is low, we modified Equation (1) by adding a dependency on the hourly rainfall intensity at the time step of the simulation (Equation (2)):
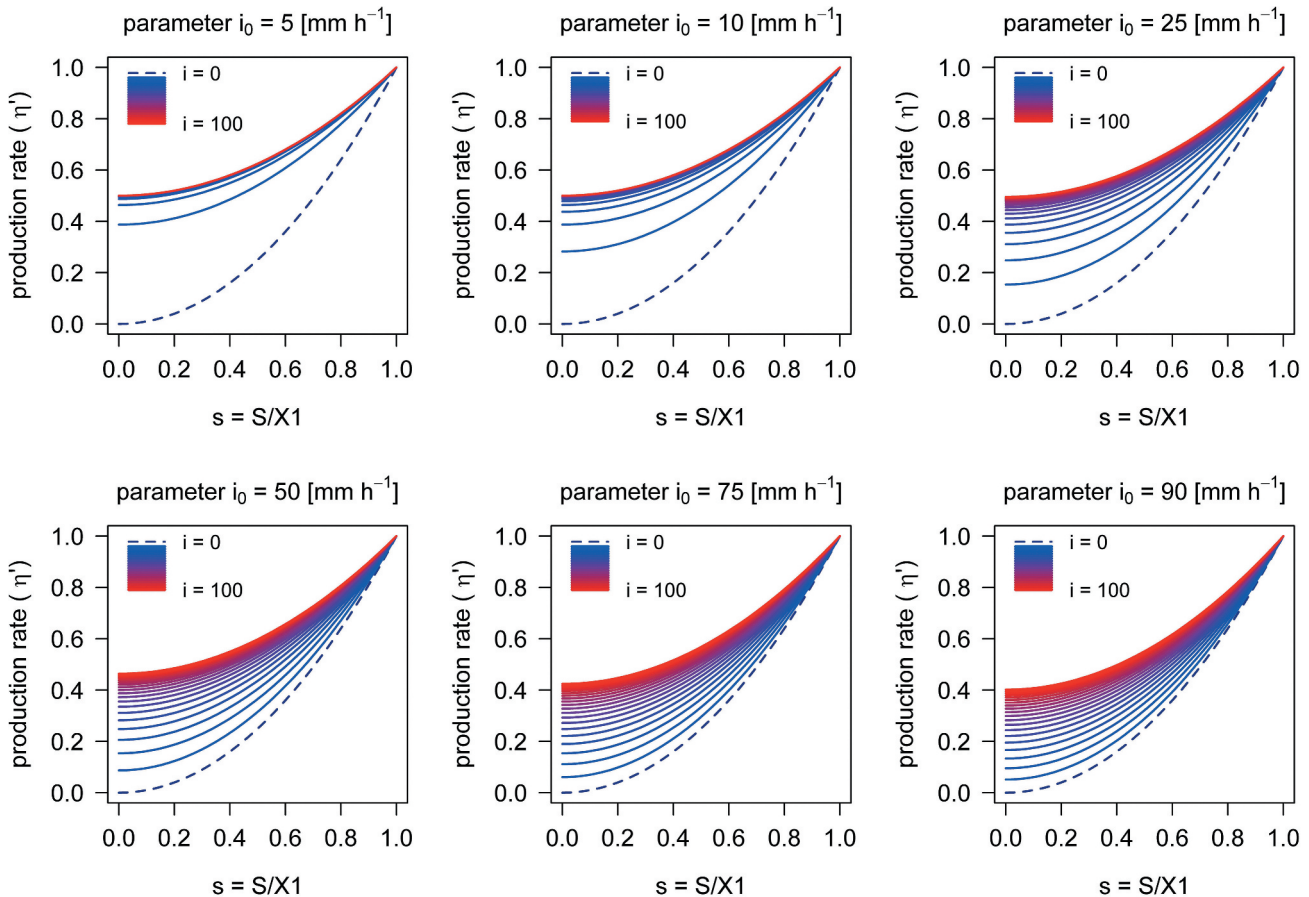
Figure 2. Evolution of the rainfall production rate for six values of the parameter i_0 [mm h^{-1}] and observed values of rainfall intensity (i) from 0 [mm h^{-1}] to 100 [mm h^{-1}] in steps of 5 [mm h^{-1}]. The horizontal axis represents the production rate obtained with the relation $s = S/X_1$, and the vertical axis represents the production rate obtained with Equation (2). Dashed lines represent the production rate obtained with Equation (1), which equals the production rate obtained with Equation (2) and $i = 0$ [mm h^{-1}].

$$\eta' = \frac{s^2 + 1 - exp\left(-\frac{i}{i_0}\right)}{2 - exp\left(-\frac{i}{i_0}\right)} \qquad (2)$$

where η' is the modified production rate; i_0 [mm h^{-1}] is the characteristic rainfall intensity (new free parameter to be calibrated; Table 1); s [-] is the production store rate, defined as the level (S) divided by the store capacity (parameter X_1); and i [mm h^{-1}] is the observed rainfall intensity at the hourly time step.

The parameter i_0 controls the response of the function to the rainfall intensity. The behaviour of the adapted production rate curves will be closer to that of the original curve as the i_0 value increases (i.e. Equation (2) turns back to Equation (1)). Figure 2 illustrates this behaviour. It shows the evolution of the modified production rate for different values of rainfall intensity i [0; 90] [mm h^{-1}], at steps of 5 [mm h^{-1}], and parameter i_0 [5; 10; 25; 50; 75; 90] [mm h^{-1}]. Assuming that a non-saturated soil could be represented by a low production store rate, if the observed rainfall intensity is low (below the lower blue curve of $i = 5$ [mm h^{-1}]), the behaviour of the production rate curves with the modified equation (Equation (2)) is equal to the original curve of the GRSD model (Equation (1)), which is given by the dashed line (similar to using $i = 0$ [mm h^{-1}] in Equation (2)).

For a given low production store rate, as the observed rainfall intensity becomes higher (i.e. blue curves move towards red curves), the modified production rate equation gives higher rates of production than the original function, despite the non-saturated conditions of the production store. On the other hand, if saturation is high (meaning an almost filled production store), the curves obtained from the original and the modified equations for the production rate converge, especially for higher intensities, giving similar values for the production rate. This feature ensures that the original behaviour of the production function of the GRSD model is maintained when the production store levels are high. It also offers more flexibility to the model to simulate high flows and floods under different forcing and model internal state conditions of the production store. Finally, we note that the production rate obtained with Equation (2) will never exceed a value of 0.5, reached when the production store is empty. This behaviour is inherent to the construction of the equation. It allows at least 50% of net rainfall to fill in the production store when it is empty.

2.3 Model setup, calibration and validation strategy

GRSD and GRSDi models simulate streamflow continuously at the hourly time step. For the spatial discretization, we adopted modelling units with a target size of 50 km^2 within each sub-catchment with a gauging station at its outlet. The choice of spatial resolution depends on the typical spatial extent of rainfall events, or on the spatial correlation length of hourly accumulated rainfall. Obled *et al.* (2009) suggest to take into consideration the maximum spatial resolution over which the rainfall can be averaged (i.e. considered uniform in space) to define the size (or number) of modelling units or sub-catchments of a semi-distributed model. Given the

dependency of the rainfall spatial correlation to the time step of the rainfall accumulation, and based on the most common theoretical variogram models applied in geostatistical analyses of rain fields, Obled *et al.* (2009) indicate that for the most intense rainfall events (often convective rain events), the range of spatial decorrelation can be estimated to be between 18 and 25 km for one-hour rain accumulations. The authors recommend considering a maximum spatial discretization lying between 150 and 300 km^2. In our case, also given the size of the sub-catchments (under 150 km^2, see Section 2.4), a target size of 50 km^2 was selected for the modelling units. This allows us to capture well the rainfall spatial variability within the smaller sub-catchments without creating modelling units that are too small and would just increase computational time without bringing additional value to model performance.

Each model is calibrated separately, against observed discharges. The calibration algorithm relies on a systematic inspection of the parameter space followed by a local search procedure, as described in Coron *et al.* (2017). There can be one or several modelling units upstream of a gauged sub-catchment. The set of calibrated parameters obtained for a gauged sub-catchment is associated to each modelling unit within its area, with the exception of the time parameter X_4. This parameter is unique for each modelling unit, since it is scaled by the area of each modelling unit. Calibration was performed sequentially (de Lavenne *et al.* 2019), from the most upstream sub-catchments to the downstream sub-catchments. The Kling-Gupta Efficiency (KGE) criterion (Gupta *et al.* 2009, Equation (3)) was used to select the best parameter set during calibration and to evaluate model performance during calibration and validation:

$$KGE = 1 - \sqrt{(r-1)^2 + (\alpha-1)^2 + (\beta-1)^2} \qquad (3)$$

where r is the linear correlation between observed and simulated discharges, α is a measure of the discharge variability error (ratio of standard deviations) and β is a bias component (ration of mean discharges).

A spatial cross-validation was performed, where the available gauged stations are separated into two complementary datasets. Calibration outlets are included in the calibration, while validation outlets are only used to validate the model after calibration. The choice of calibration and validation outlets depends on various issues: availability of long time series for robust calibration, quality of discharge data, representativeness of the gauged points inside the catchment, and typical location of intense rainfall events, among others. In this study, we used about 50% of the gauged outlets for calibration (Fig. 3). In the selection, we sought to benefit from having discharge information distributed over the whole catchment area.

2.4 Study area

The models were evaluated over the Aude catchment, located in southwest France (Fig. 3). It has a total drainage area of 6074 km^2, extending from its most upstream areas draining from two mountainous regions (the Corbières Mountains and the Pyrénées Massif in the southwest, and the Montagne Noire in the north) to the Mediterranean Sea. In this study, the delta
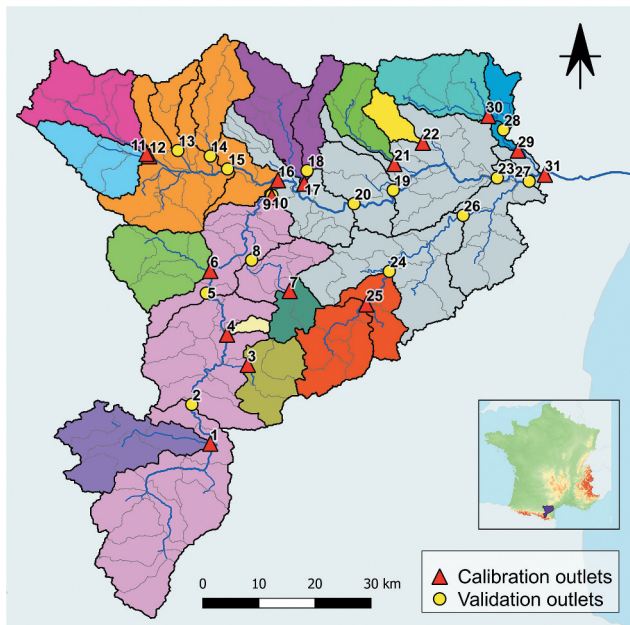
Figure 3. Location of the Aude catchment in France, showing the river network and the outlets used for model calibration (16 stations, red triangles) and validation (15 stations, yellow circles). The calibrated sub-catchment areas are represented in different colours. The 109 modelling units inside the sub-catchments are shown in grey contours. Their sizes range from 11 to 65 km², with a median size of 45 km².

part of the catchment is excluded and the modelled area extends down up to the Moussoulens station, which represents a drainage area of 4840 km² (outlet 31, Fig. 3). The soils are mostly of silty and sandy composition, with rock types that are limestones and calcariferous molasse. A few areas in the Montagne Noire region are karstified (Gaume *et al.* 2004).

The climate of the Aude catchment is characterized by its geographical contrasts. In the northern and southern regions, it is a mountainous climate (about 10% of the total catchment area), while the western regions display a temperate oceanic climate. A dominant Mediterranean climate is found in the downstream part of the catchment, characterized by the occurrence of thunderstorms in autumn, and hot and dry summers. Mean annual precipitation over the Aude catchment is 860 mm (1970–2010). The hydrological regime reflects its contrasting climate. It is nivo-pluvial in the upstream mountainous sub-catchments and Mediterranean for the downstream parts of the catchment and its tributaries. The combined influence of mountainous regions and the closeness to the Mediterranean Sea leads to floods that may occur at different times of the year. In autumn, floods are often the result of short-duration, stationary convective rainfall generated by warm wet masses of air coming from the sea. Floods in winter and spring are often the result of moderate but persistent rain, resulting in high accumulations.

2.5 Hydrometeorological data

Precipitation data come from the quantitative precipitation estimates of the ANTILOPE J+1 product by Météo-France for the period from 1 January 2008 to 18 October 2018.

These estimates are available at the hourly time step and a - 1 × 1 km grid resolution. ANTILOPE J+1 data are the result of radar measurements corrected with rain gauge observations (Laurantin 2008, Champeaux *et al.* 2009). Evapotranspiration was estimated using the Oudin formula (Oudin *et al.* 2005) and the temperature data provided by the SAFRAN meteorological reanalysis produced by Météo-France on an 8 × 8 km square grid (Vidal *et al.* 2010). Gridded data were averaged over the modelling units by overlaying the data grids with the modelling units' boundaries.

Hourly discharge data were extracted from the French Hydro database (Leleu *et al.* 2014) for 31 stations over the 2008–2018 period. Except for the most downstream station (4840 km²), sub-catchment areas vary from a minimum size of 15 km² to a maximum of 4600 km² (outlets 4 and 27, respectively; Fig. 3). Not all hydrometric stations have continuous data for the study period; however, the amount of missing data never exceeds 10% of the total period. Some discharge data are slightly influenced by hydropower dams along the upstream parts of the main river and by two navigation channels: the Canal du Midi, which crosses the northern part of the catchment from west to east, and the Canal de la Robine, which is connected to the main river downstream and flows directly to the Mediterranean Sea. There are also withdrawals of water mainly for agriculture and for drinking water supply around the city of Carcassone. Human influences, however, affect mainly the low flow periods, which are not the focus of this study. Hydrometric stations were separated into two groups for model calibration (16 outlets) and validation (15 outlets). Their location and the spatial discretization of the catchment area, producing a total of 109 modelling units, are also presented in Fig. 3. Furthermore, snowmelt processes were not taken into account in the models since snowmelt is not the main flood-generation mechanism. Solid precipitation does not exceed 10% of the annual precipitation over the study period.

2.6 Flood event selection and event-based evaluation

Besides evaluating the performance of the models for the whole data period (2008–2018), we also focused on four selected flood events. To select the events, we first extracted the 10 highest peak discharges within the calibration period for each sub-catchment with a gauged station. Common events affecting at least two thirds of the 31 gauged stations, within a time window no longer than four days, were selected to allow a larger number of data locations in the evaluation. Only four events satisfied these conditions and they took place in different seasons of the year and in recent years, allowing us to assess the flexibility brought by the adaptation incorporated in the model structure: one spring event (15–17 March 2011), one winter event (13–15 February 2017) and two autumn events (28 November–1 December 2014; 14–15 October 2018). These events also vary in terms of Soil Wetness Index (SWI), an index provided by the Interaction Sol-Biosphère-Atmosphère (ISBA) model in the Système d'Analyse Fournissant des Renseignements Adaptés à la Nivologie (SAFRAN) reanalysis (Vidal *et al.* 2010). Its value varies mainly between 0 (extremely dry soil) and 1 (extremely wet soil). Below 0.5 a soil is

considered to be dry, and above 0.8 it is considered very wet (Habets *et al.* 2008). The average values over the Aude catchment on the day before the start of each event are 0.93 for the spring 2011 event, 0.75 for the winter 2017 event, 0.43 for the autumn 2014 event and 0.51 for the autumn 2018 event.

The spring 2011, winter 2017 and autumn 2014 flood events triggered the third level (out of four) of the French flood alert system "Vigicrues" (risk of flood generating major overflows likely to have a significant impact on community life and the safety of property and people). The most extreme event was the one in autumn 2018. It triggered the highest level of flood warning (risk of major flooding; direct and widespread threat to the safety of people and property). Table 2 shows some key characteristics of the four selected events. The autumn events (E3 and E4) have the highest values of observed catchment-averaged rainfall intensity in one hour. The October 2018 event (E4) is not only the event that occurred in almost all of the gauged sub-catchments, but also the one that has the highest specific peak discharge. The spring (E1) and winter (E2) events show similar observed rainfall intensities, but the winter event has a more moderate specific peak discharge and affected fewer sub-catchments. Fig. 4 shows the different spatial distributions of the accumulated rainfall of each event, with up to 300 mm of point rainfall given by the ANTILOPE J+1 gridded data.

The differences in rainfall distribution and flood severity among the selected events allow us to have a closer look at the differences in the performance of the GRSD and the GRSDi models under different situations. To evaluate the models, two event-based criteria were applied to the selected events: one that quantifies errors in peak discharge values (ΔQ [-], Equation (4)) and another that quantifies errors in the timing of the peak discharges (Δt [h], Equation (5)):

$$\Delta Q = \frac{Q_{sim} - Q_{obs}}{Q_{obs}} \quad (4)$$

$$\Delta t = t_{sim} - t_{obs} \quad (5)$$

where Q_{sim} [m³ s⁻¹] and Q_{obs} [m³ s⁻¹] are the simulated and the observed peak discharges, respectively, and t_{sim} [h] and t_{obs} [h] are the simulated and observed peak times, respectively.

Table 2. Characteristics of four selected flood events in the Aude catchment: number of catchments affected (out of 31), study period for each event, I_{max} (maximum catchment-averaged hourly rainfall intensity, with corresponding outlet) and Q_{max} (maximum specific peak discharge, with corresponding outlet). Outlet numbers are shown in Fig. 3.

Event	No. of catchments reacting over 31	Event study period	I_{max} [mm h⁻¹] (outlet)	Q_{max} [m³ s⁻¹ km⁻²] (outlet)
E1	24	15/03/2011 0 h–17/03/2011 23 h	12 (30)	2.17 (28)
E2	20	13/02/2017 0 h–15/02/2017 23 h	17 (21)	1.77 (18)
E3	22	28/11/2014 0 h–01/12/2014 23 h	31 (22)	2.61 (7)
E4	29	14/10/2018 0 h–15/10/2018 23 h	35 (7)	6.65 (7)

3 Results

This section presents the long-term and event-based evaluation of the performance of the GRSDi model, as well as the results of the analysis of model versatility. It is important to keep in mind that the adaptation proposed in the model aims to bring improvements to specific flood events, without, however, deteriorating the long-term and overall performance of the original GRSD model structure.

3.1 Long-term performance of the models

The performance of the GRSD model over the period 2008–2018 is presented in Fig. 5. We obtain a mean KGE of 0.87 at the calibration outlets and 0.62 at the validation outlets. Only one validation outlet (number 8) displays low performance, which was mainly due to the model's tendency to overestimate low flows at this outlet (KGE bias component of around 1.8). For the GRSDi model, we obtain a mean KGE of 0.88 at the calibration outlets and 0.63 at the validation outlets.

Figure 6 shows the differences in KGE values between the models for each outlet. Absolute differences in performance are smaller than 0.1, with positive differences (better KGE for GRSDi) occurring more often. These results show that the new model structure does not deteriorate model simulations obtained from the original model structure. Improvements in the southern part of the catchment are fewer, which could be because this area is less affected by the flood events that the GRSDi model tries to tackle.

3.2 Impact of the GRSDi model dependency on rainfall intensity on the simulation of flood events

Figure 7 shows the simulated and observed discharges for the four events described in Section 2.6 at four outlets (20, 18, 21 and 22) that are representative of the sub-catchments' responses for each event. Table 3 shows the differences in peak flow (ΔQ) and time of peak (Δt) between simulated and observed discharges for these outlets. The event-based assessment shows that both models simulate well the observed discharges for the events occurring in spring (E1) and winter (E2). Differences in peak flow are between +3% and +11% of the observed peak discharges (Table 3). For the floods occurring in autumn (E3 and E4), the GRSD model clearly underestimates the peak discharges, with differences in peak flows (ΔQ) of −73% and −53% of the observed peak discharges. These differences are much smaller for the GRSDi model: +14% and −20% for E3 and E4, respectively. In terms of time of the peak discharge, the GRSD and GRSDi model simulations do not differ for the winter event (E2). The longest event (E1) has its peak discharge simulated two hours before the observed peak by the GRSDi model and one hour by the GRSD model (Outlet 20; Table 3). For the autumn events (E3 and E4), GRSD simulates peak discharges one hour after the observed peaks, while GRSDi shows the right timing in its simulations. The small differences in time of the peak discharge between the two models are expected since the modification of the production function does not directly affect the routing part of the model.
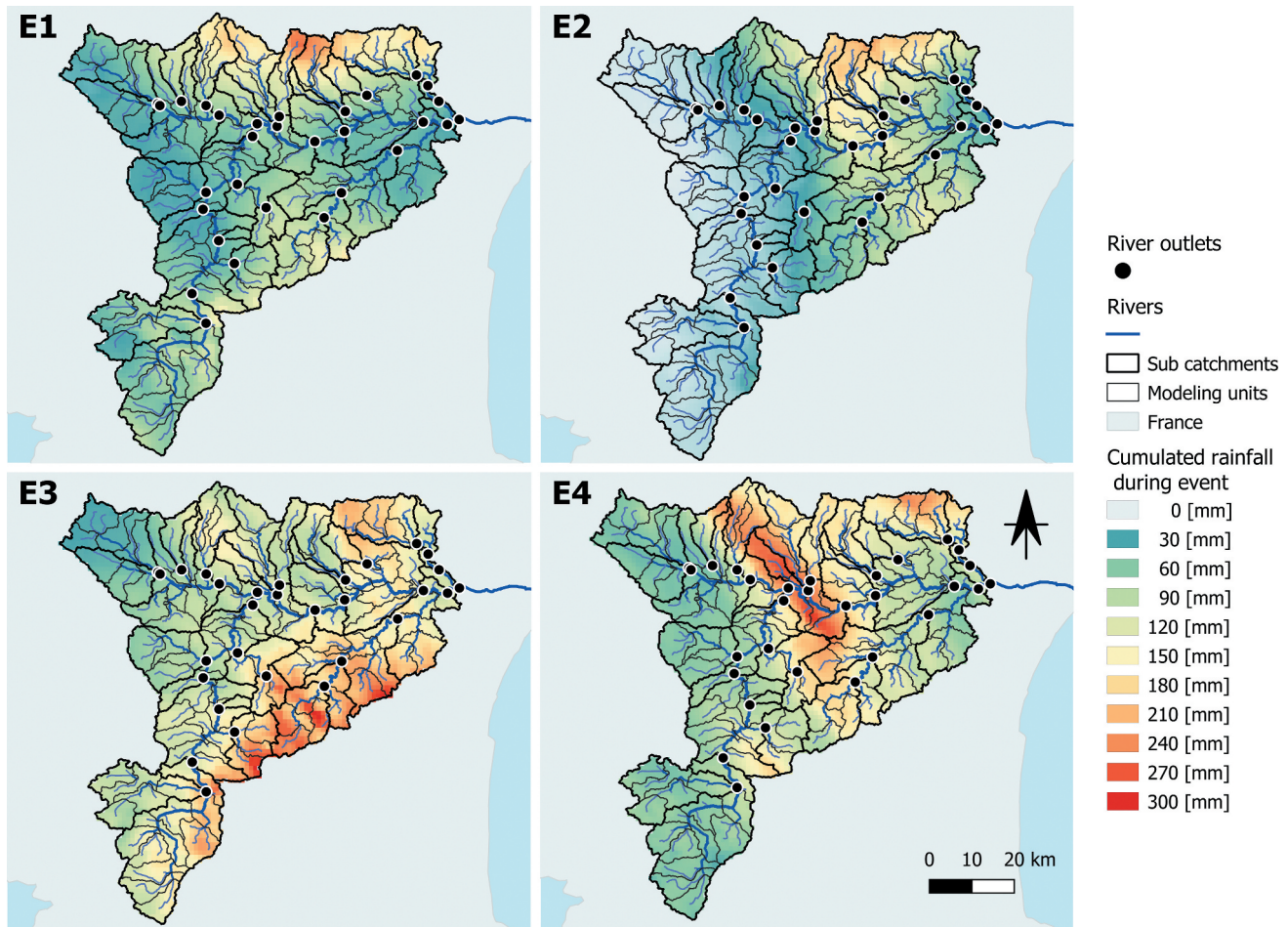
Figure 4. Cumulative rainfall [mm] for four events in the Aude catchment. E1: 15/03/2011 0 h–17/03/2011 23 h; E2: 13/02/2017 0 h–15/02/2017 23 h; E3: 28/11/2014 0 h–01/12/2014 23 h; E4: 14/10/2018 0 h–15/10/2018 23 h. Data source: ANTILOPE J+1 product from Météo-France.
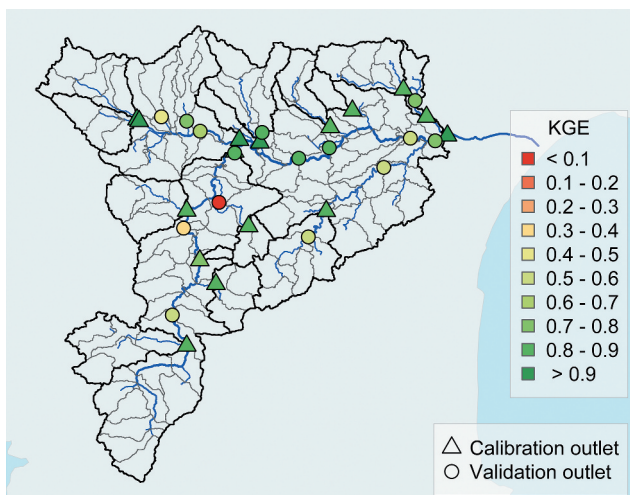

Figure 5. KGE values for the GRSD model at 16 calibration outlets and 15 validation outlets. Period: 01/10/2008 0 h–18/10/2018 23 h.
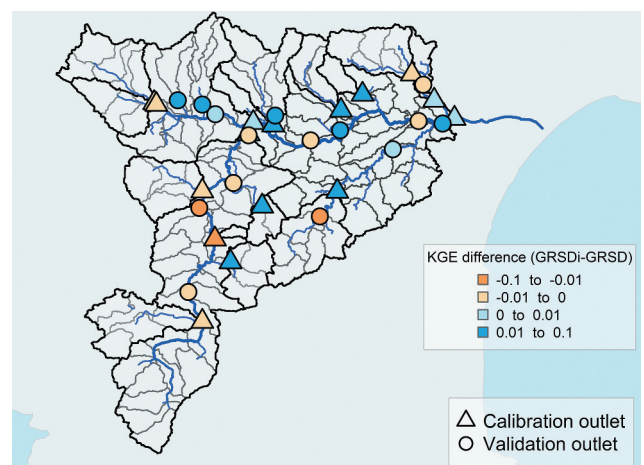

Figure 6. Difference in KGE values between the GRSDi and the GRSD models at 16 calibration outlets and 15 validation outlets. Period: 01/10/2008 0 h–18/10/2018 23 h.

Figure 8 shows the evaluation criteria *ΔQ* and *Δt* of one model (GRSDi, on the y-axis) against the other model (GRSD, on the x-axis) for all outlets that showed a hydrological response to the rain events. When the GRSDi simulations perform better than the GRSD simulations, the points are situated in the lower sides of the cross-sections (blue areas below the diagonals) in quadrant I and II, and in the upper sides of the cross-sections (blue areas above the diagonals) of quadrant III and IV. If the models perform equally, the points are aligned along the diagonals. If both models perform "perfectly," for these criteria, the points are located in the centre (0, 0). We can see that, in general, when points are located
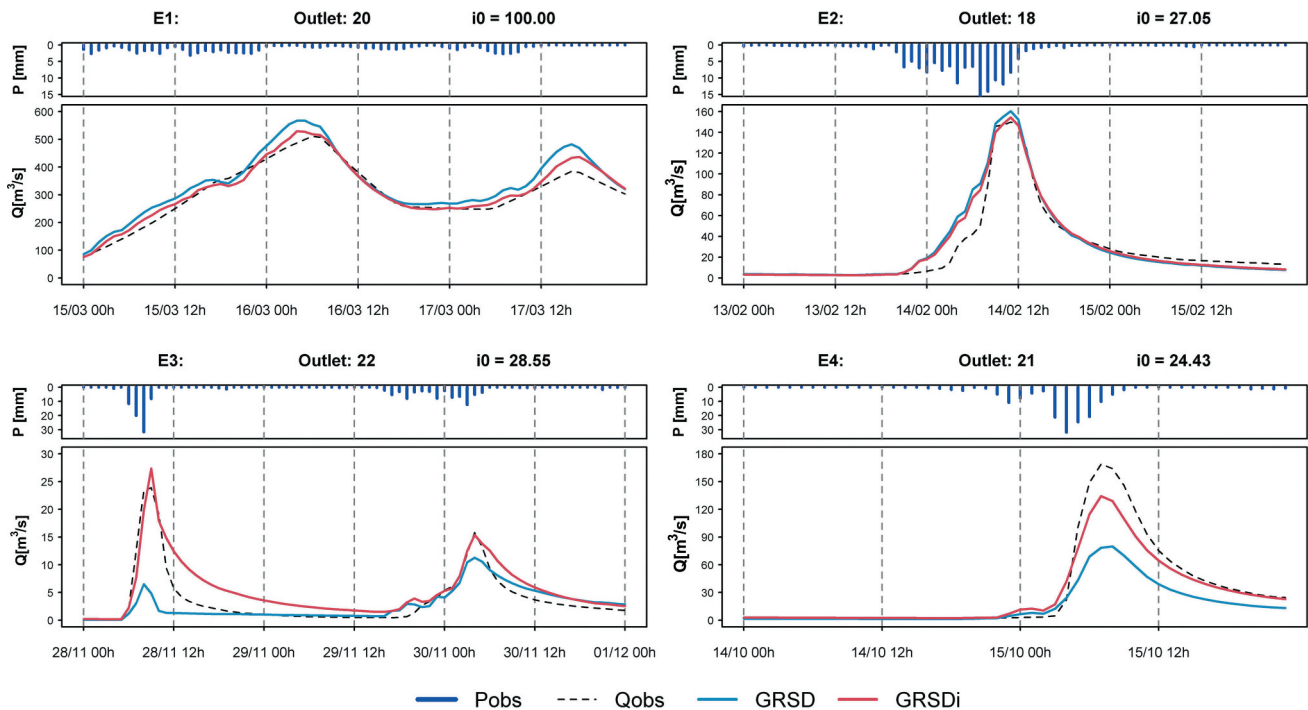
Figure 7. Hydrographs of observed (Q_{obs}) and simulated (GRSD and GRSDi models) discharges for the four selected flood events (E1 to E4; see Table 2) and selected outlets. Observed catchment-averaged rainfall (P_{obs}) is shown in the upper panels of each hydrograph, as well as the characteristic rainfall intensity (i_0) parameter of the GRSDi model. Wetter soil conditions precede the E1 (spring) and E2 (winter) events; drier soil conditions precede the E3 and E4 (autumn) flood events.

Table 3. Differences in peak flow (ΔQ) and time of peak (Δt) between simulated (GRSD and GRSDi models) and observed discharges for the four selected events (E1 to E4; see Table 2) and selected outlets.

	E1 (Outlet 20)		E2 (Outlet 18)		E3 (Outlet 22)		E4 (Outlet 21)	
	GRSD	GRSDi	GRSD	GRSDi	GRSD	GRSDi	GRSD	GRSDi
ΔQ [-]	0.11	0.04	0.07	0.03	−0.73	0.14	−0.53	−0.20
Δt [h]	−1	−2	0	0	1	0	1	0

farther from the centre, they have a tendency to be aligned close to the diagonals (i.e. very bad performance is equally bad for both models; red areas) or to show the same tendency for the deviations in peak flows and time of peak (i.e. points tend to remain in quadrants I and III), even if the magnitudes of the deviations are slightly different. In terms of Δt, the GRSDi tends to perform better than or equal to GRSD. Differences in performance (points far from the diagonal) are more often observed in the evaluation criterion ΔQ. For E1 and E2, GRSDi tends to increase (or decrease) the percentage of overestimations (or underestimations) of the peak flows, although the points remain, in general, close to the diagonal crossing quadrants I and III. For E3, overestimations were reduced with the use of GRSDi, while underestimations were either reduced or increased, depending on the outlet. For E4, about two thirds of the outlets show better performance for the GRSDi model, with underestimation ($\Delta Q < 0$) reduced. The percentage of overestimation increased in about seven outlets. A visual inspection of the hydrographs revealed that these are outlets that show a very moderate to low response to the rain event.

In order to visualize where the performance of the GRSDi model is worse or better than the performance of the GRSD model, based on the outlets shown in Fig. 8, we present the maps

that result from comparing ΔQ and Δt values (Figs 9 and 10, respectively) between the two models for the four selected events. Outlets coloured in blue (pink) represent points where GRSDi outperforms (underperforms) GRSD. Outlets in grey indicate similar performance and the same sign (i.e. close values of ΔQ, with both models under- or overestimating observed discharges, and the same deviations for Δt, with both models in advance or both with a delay with regards to the observed peak discharges). Outlets in yellow indicate similar performance but opposite signs (i.e. for ΔQ, one model underestimates while the other overestimates by close values of the criterion; for Δt, one model has a delay equal to the advance of the other model). The maps also indicate whether an outlet was used in model calibration or left for validation.

Figure 9 shows that GRSDi performs better than GRSD at most outlets for the autumn events (E3 and E4). For E3, GRSDi is the best model at 13 out of 22 stations, including all calibration and validation outlets that showed a hydrological response to the rain event. For the most extreme event, E4, GRSDi outperforms at 16 out of 28 stations. The highest losses in performance for the GRSDi model for this event (October 2018) are located in the downstream part of the catchment, where the original GRSD model already overestimates the observed discharges. Overestimations in the downstream outlets can be explained by a lamination effect in the observed discharges, given the magnitude of the event and the flooding that occurred during the event (which is not simulated by the hydrological model). For the spring 2011 event (E1), GRSDi is best at 14 out of 24 stations. Lower performance is seen at 10 outlets (five of them used for calibration). The winter event (E2) shows GRSDi is the best model at seven out of the 19 stations that showed a hydrological response to the rain event. In the remaining 12 stations, differences in ΔQ
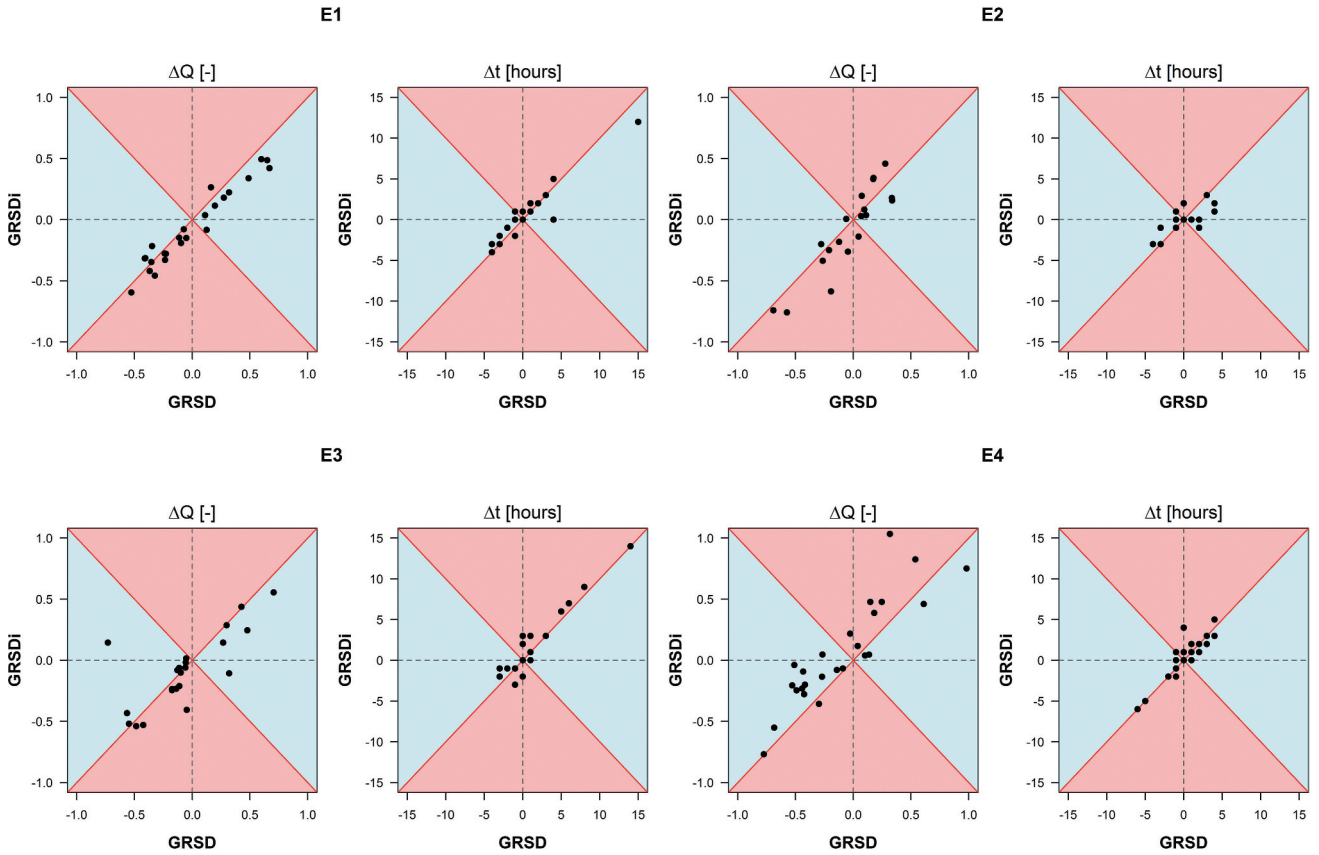
Figure 8. ΔQ and Δt values for GRSDi (y-axis) and GRSD (x-axis) models for four selected events (E1 to E4; see Table 2) and all the outlets of the Aude catchment. Points in the blue (red) areas indicate better (worse) performance for the GRSDi model. Points aligned along the diagonals (in the 0,0 centre) indicate equal (perfect) performance for both models.

remain low, and we observe that peak discharges were already underestimated in the simulations with the original GRSD model structure. For all events, outlets showing improvements with the use of the GRSDi model are mostly located in the areas of highest cumulated rainfall and along the main river (Fig. 4).

Figure 10 shows the same comparison between models, but for the criterion Δt. For the spring event (E1), similar performance among models is more often observed (10 out of 24 stations, with three stations providing similar performance but with the opposite sign of the criterion), followed by best performance by GRSD (seven stations, located mostly downstream of the catchment). For the winter event (E2), all 19 outlets but for one validation outlet show either better performance with GRSDi (11 outlets) or similar performance between models (seven outlets, with either the same or opposite sign). The event of autumn 2014 (E3) shows GRSDi is best or has similar performance at 14 out of 22 stations. For the October 2018 event (E4), GRSDi performs better at seven out of 28 stations, and similarly at 14 stations (nine with the same sign of Δt and five with the opposite sign). Losses in performance are located mostly in the northwestern part of the catchment, where the original GRSD model already shows difficulties in performing well. Again, most of the improvements with the GRSDi model are located in the areas of high cumulated rainfall. For the 2014 event (E3) only, outlets located in these areas have either similar performance or better performance for the GRSD model.

3.3 Model versatility in a continuous simulation and influence of the parameter i_0

To investigate how the adaptation proposed with the GRSDi model is activated (or not) during a continuous simulation of river flows, we built a visualization tool to detect the time steps within the simulation period when the model tends to behave like the original GRSD model structure, and the time steps when it brings up front the benefits of the adaptation proposed with the GRSDi structure. The shift in behaviour can be investigated by examining the differences in runoff production (P_r) in the modelling units of the catchment. We first calculate the absolute values of this difference (Equation (6)) and then we identify the time periods when the results show the highest differences.

$$\Delta R = |Pr_{GRSDi} - Pr_{GRSD}| \qquad (6)$$

where ΔR is the difference in runoff production, Pr_{GRSDi} is the runoff production of GRSDi model and Pr_{GRSD} is the runoff production of GRSD model.

Figure 11 shows an example of two modelling units situated inside two sub-catchments with a calibration outlet. We selected modelling units with complete discharge time series for the period 2008–2018 that are located in areas of high cumulated rainfall for all four selected events. To illustrate differences in behaviour according to the values of the parameter i_0, we selected a modelling unit with a high value of i_0 (100 mm h^{-1}) and a modelling unit with a low value of i_0 (28.5 mm h^{-1}). We also show: (a) a modelling unit
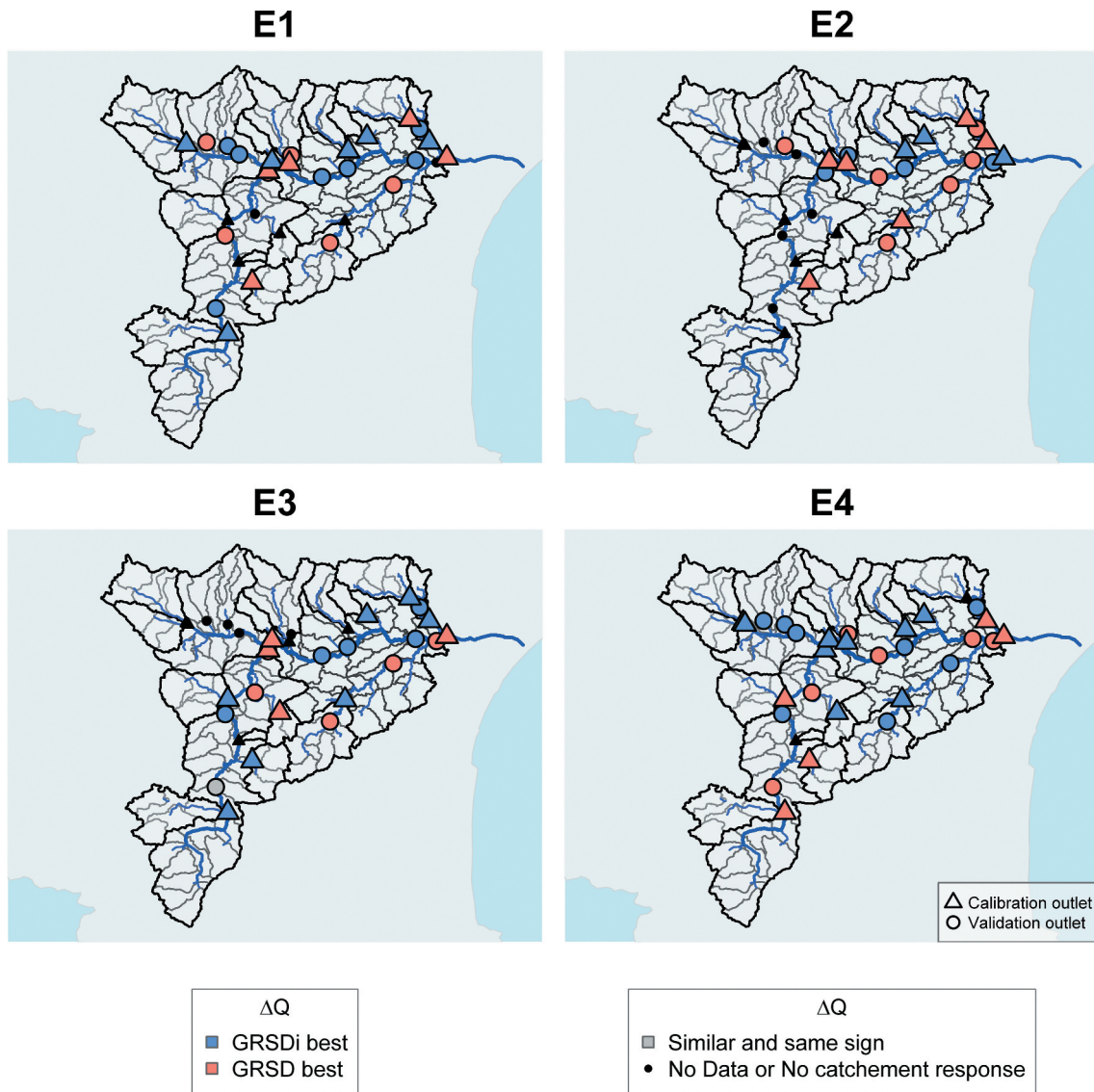
Figure 9. Location and comparison of performance in terms of ΔQ values with GRSD and GRSDi models for all the outlets within the Aude catchment and the four selected events (E1 to E4; see Table 2). Outlets in black either have missing data during the event or show no significant hydrological response to rainfall. GRSDi (GRSD) best: the simulated peak discharge from the GRSDi (GRSD) model is closer to the observed peak discharge. Similar and same sign: both models similarly underestimate or overestimate the peak discharge, with a difference in ΔQ lower than 0.1.

contributing to an outlet that shows better overall performance (KGE value) for the GRSD model, and (b) a modelling unit contributing to an outlet that shows better overall performance for the GRSDi model. Figure 11 displays four panels that show the evolution of the observed areal rainfall over the modelling unit, the filling rate of the production store, obtained by dividing its level S by its maximum capacity X_1 at each time step (S/X_1), the differences in runoff production for both models, and a stripe-based graph, where the stripes represent four intervals of the absolute differences in runoff. For the intervals, we considered that any difference in runoff production lower than or equal to 0.5 [mm h^{-1}] is equivalent to no difference (ND). These occurrences represent 99.8% of all differences from all 109 modelling units and all 87 863 time steps of the analysis. Low (L), medium (M) and high (H) differences are then defined based on percentiles of the remaining values. Low differences are values greater than 0.5

[mm h^{-1}] and less than or equal to the 50th percentile (median); median differences are greater than the median and less than or equal to the 75th percentile; high differences are greater than the 75th percentile.

The parameter i_0 varies within the interval [0; 100] [mm h^{-1}] and, given the behaviour of the production rate curves (Fig. 2), the closer the calibrated value is to 100 [mm h^{-1}], the more the GRSDi model behaves like the original GRSD model in terms of runoff generated by the production function. This is illustrated in the case shown in Fig. 11(a). The production rate will seldom be adjusted as a function of the hourly observed rainfall intensity. There are thus more times steps at which there is no difference (blank stripes) between the values of runoff production of the two models. In the opposite situation, as illustrated in Fig. 11(b), the smaller the calibrated value of i_0, the more the model will make use of the adapted GRSDi production rate, as a function of the rainfall intensity.
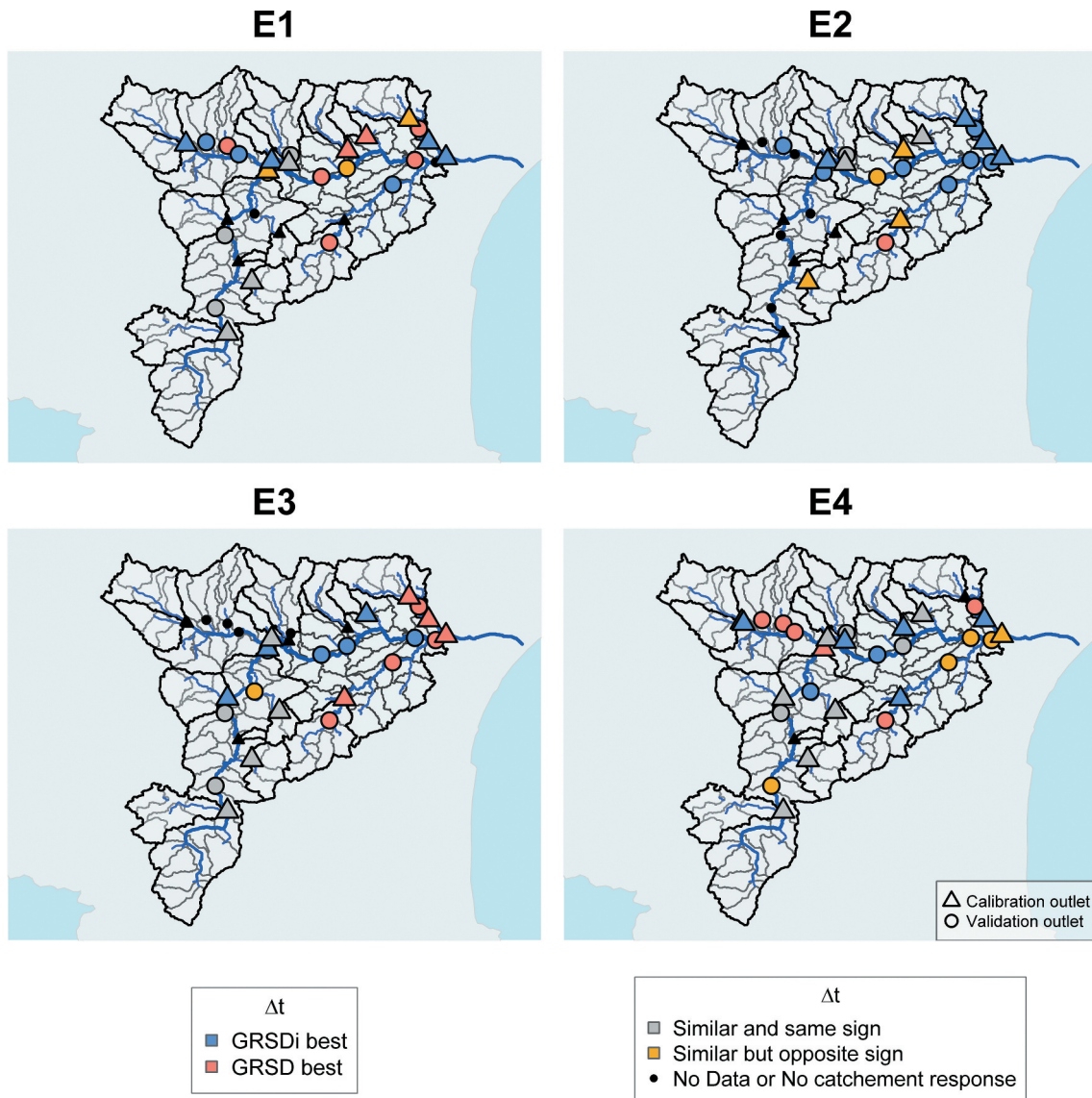
Figure 10. Location and comparison of performance in terms of Δt values with GRSD and GRSDi models for all the outlets within the Aude catchment and the four selected events (E1 to E4; see Table 2). Outlets in black either have missing data during the event or show no significant hydrological response to rainfall. GRSDi (GRSD) best: the time of the simulated peak discharge from the GRSDi (GRSD) model is closer to the time of the observed peak discharge. Similar and same sign: the models present the same time deviations, with both in advance or with a delay. Similar but opposite sign: the models present the same time deviations, but one in advance and the other with a delay.

In these situations, differences in runoff will be more frequent over the time period of the analysis. We note that, even if differences in model behaviour are less frequent when the parameter i_0 reaches its upper bound (Fig. 11(a)), they are not inexistent. This may suggest that this limit may not be enough and that it would benefit the GRSDi model if a higher value could be reached during calibration.

The differences in the runoff production of both models are higher (differences in red in Fig. 11, bottom panels) mostly when the level of the production store (middle upper panels) is low at the time steps before high rainfall intensities (top panels). This corresponds well to the goal of the modification introduced with the GRSDi model, with regard to the original structure of the GRSD model. For high values of parameter i_0 (Fig. 11(a)), the highest differences occur more frequently between the months of July and December. For the other half of the year, high differences are rare and there are mostly

medium to low differences. In the case of low values of parameter i_0 (Fig. 11(b)), seasonal patterns are more difficult to define since high differences appear frequently throughout the year. Nevertheless, periods of no difference occur more often in the first half of the year (mostly for the first months).

The relationships between non-zero observed rainfall and the differences in runoff production are shown in Fig. 12, which plots each time step of non-zero rainfall of the 2008–2018 period for the same modelling units as Fig. 11. The classes of differences in runoff production are also indicated. We can see that, for time steps where the rainfall intensity falls below the 80th percentile of observed non-zero hourly rainfall, almost all runoff differences can be considered negligible, falling in the no difference class of runoff production. Very high values of observed hourly rainfall (overall, values greater than 10 or 20 [mm h^{-1}], according to the modelling unit) are associated with high differences in runoff production (red
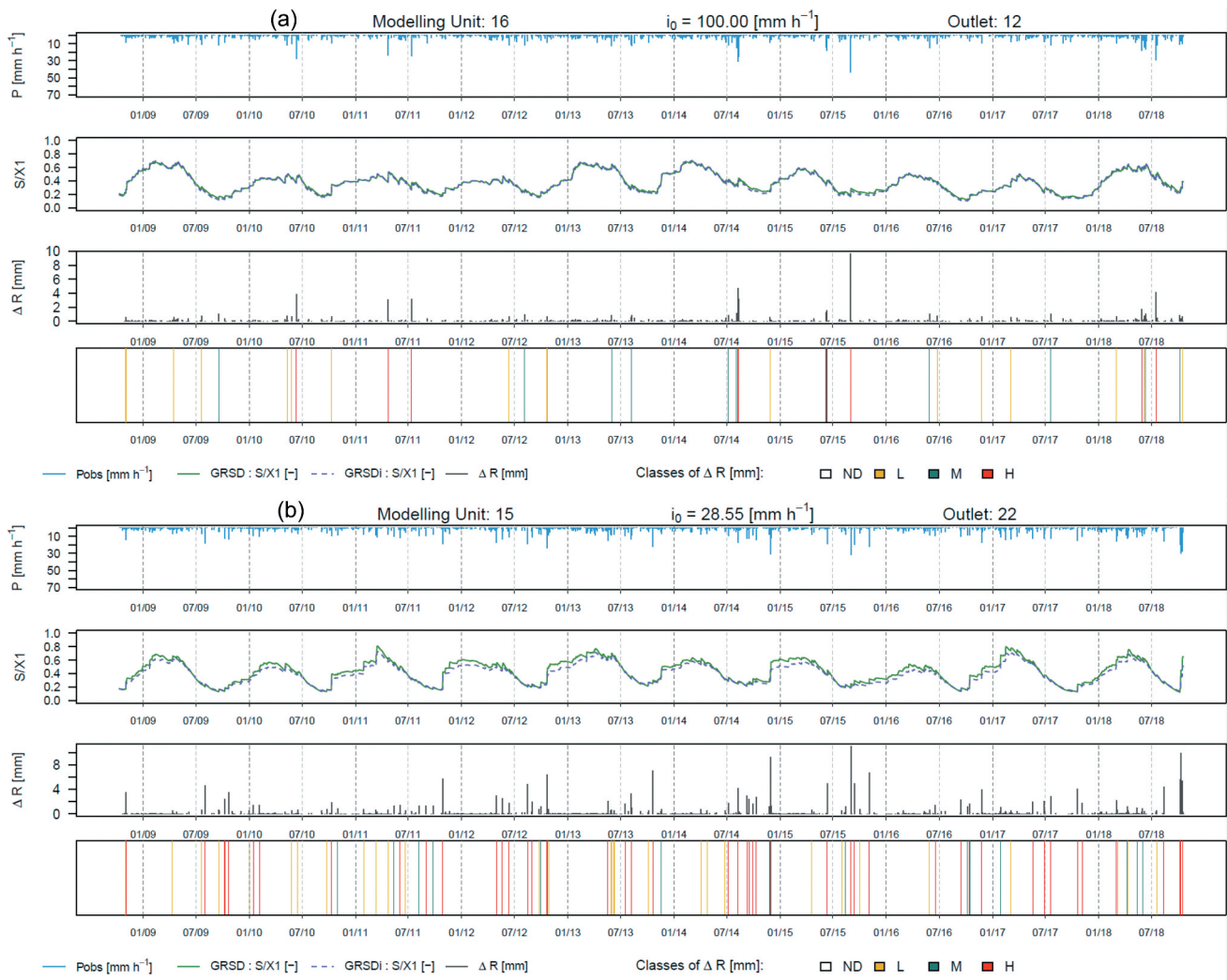
Figure 11. Illustration of model versatility for two modelling units inside two model calibration outlets; (a) has a high value of parameter i_0 and better overall performance for GRSD model, whereas (b) has a low value of parameter i_0 and better overall performance for GRSDi model. Top: observed areal hourly rainfall intensities; middle top: production rate for the GRSDi (dashed line) and the GRSD (continuous line) models; middle bottom: absolute values of relative differences in runoff production between the models; bottom: stripes of classes of differences in runoff production (ND: no difference; L: low difference; M: medium difference; H: high difference). Period: 01/10/2008 0 h–18/10/2018 23 h.
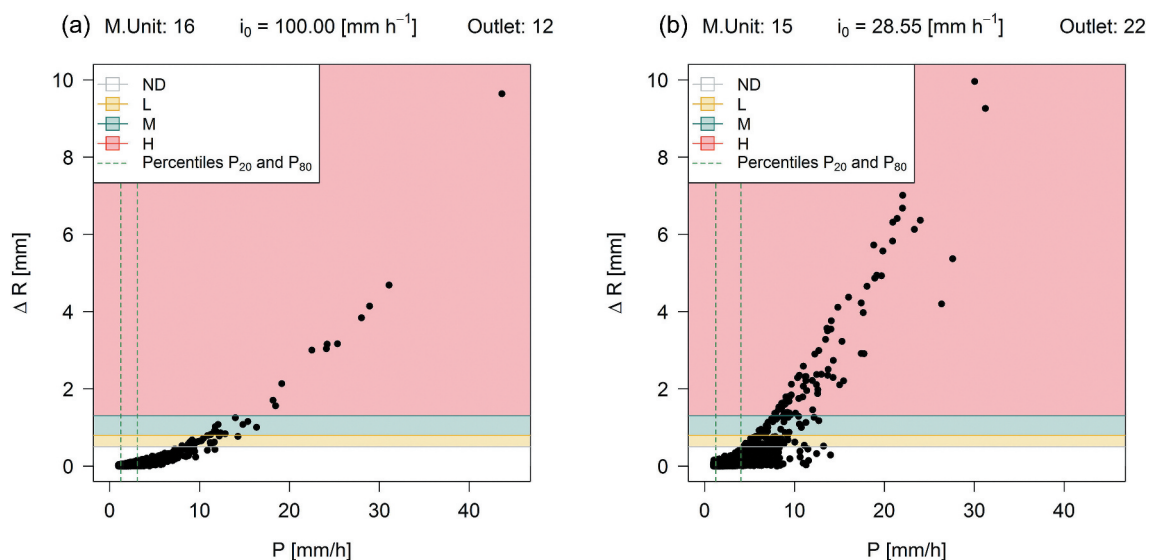

Figure 12. Differences in runoff production (ΔR) versus observed areal non-zero hourly rainfall (P) for the same modelling units as in Fig. 11. ND: no difference; L: low difference; M: medium difference; H: high difference in runoff production. The 20th and 80th percentiles (P_{20} and P_{80}) of all observed non-zero hourly rainfalls are (a) 1.2 [mm h^{-1}] and 3.1 [mm h^{-1}]; (b) 1.2 [mm h^{-1}] and 4 [mm h^{-1}].

zone in Fig. 12). The modelling unit with a lower value of the parameter i_0 (Fig. 12(b)) shows a higher exponential growth of the runoff differences with the increase of rainfall intensities. This behaviour is expected since it follows the relationship between production rate and rainfall intensity shown in Fig. 2 and Equation (2).

3.4 Model behaviour in terms of runoff generation processes

To understand the behaviour of all 109 modelling units of the study area, we analysed the differences in runoff production for different classes of rainfall intensities and levels of the filling rate of the production store that can be associated with runoff generation processes. Only time steps of non-zero rainfall during the study period were taken into account. We considered the rainfall intensities at a given time step t (in hours) and the reservoir filling rates at the previous time step $t - 1$ to separate the runoff production differences into four cases:

- Case 1 (no runoff generation condition): the observed rainfall for a given time step is low (i.e. less than or equal to the 20th percentile of all non-zero rainfall intensities)

and the filling rate of the GRSDi production store for the previous time step is also low (i.e. less or equal to the 20th percentile of all filling rates).
- Case 2 (Dunne's runoff generation): the observed rainfall for a given time step is low, but the filling rate of the GRSDi production store for the previous time step is high (i.e. greater than the 80th percentile of all filling rates).
- Case 3 (Horton's runoff generation): the observed rainfall for a given time step is high (i.e. greater than the 80th percentile of all non-zero rainfall intensities), but the filling rate of the GRSDi production store for the previous time step is low.
- Case 4 (Dunne's and Horton's runoff generation): the observed rainfall for a given time step and the filling rate of the GRSDi production store for the previous time step are high.

Modelling units were split into two groups: low parameter i_0 values [0; 50] [mm h^{-1}] (46 modelling units) and high parameter i_0 values [50; 100] [mm h^{-1}] (63 modelling units). Figure 13 shows the percentage frequency of occurrence of the differences in runoff production between GRSDi and GRSD models according to the four cases, the two groups of modelling units, and the four classes of runoff differences (ND, L, M, H). We can see that
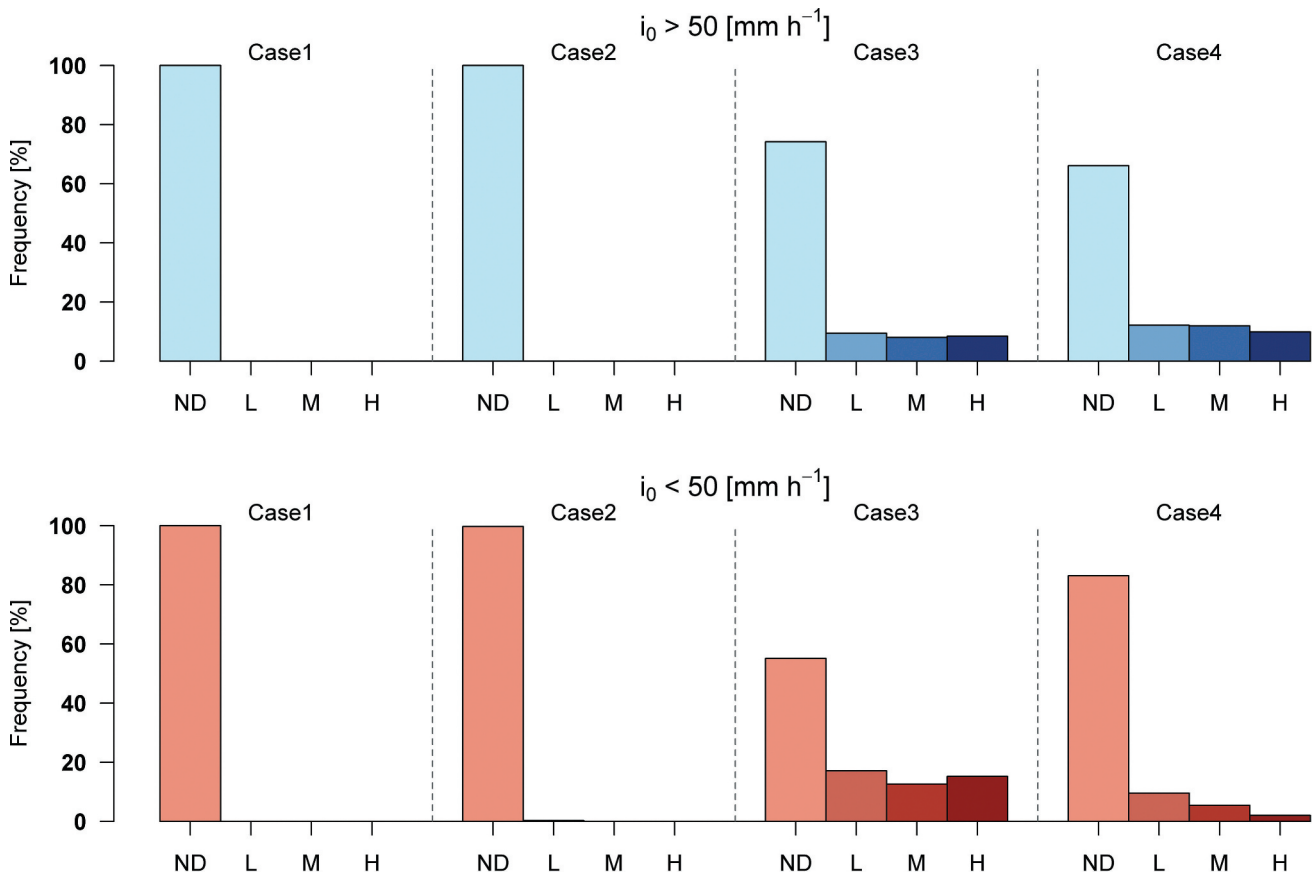

Figure 13. Percentage frequency of occurrence of the differences in runoff production between GRSDi and GRSD models according to the four cases of runoff generation (Case 1: no runoff generation condition; Case 2: Dunne's runoff generation; Case 3: Horton's runoff generation; Case 4: Dunne's and Horton's runoff generation), the two groups of modelling units (top: high parameter i_0; bottom: low parameter i_0) and the four classes of runoff production differences (ND: no difference; L: low difference; M: medium difference; H: high difference).

the class of no differences (ND) in runoff production between the models is the most frequent in all cases. This is expected as differences should appear only in cases where the adaptation introduced by the GRSDi model plays a role, which is expected to be rare (high intensities falling over dry soils). For Case 1 and Case 2, where the rainfall intensity is low, there is no occurrence of high (H) or medium (M) runoff differences, regardless of the values of the parameter i_0. Very few occurrences of low (L) differences are observed in modelling units with low parameter i_0 and high filling rate (Fig. 13, bottom, Case 2). When rainfall is high (Case 3 and Case 4), the occurrences of low, medium and high differences in runoff production between models increase in frequency. If the modelling unit has a high value of parameter i_0 (Fig. 13, top), the occurrences of non-negligible differences (L, M, H) are slightly higher when the rainfall and the filling rate are high (Case 4). When modelling units have lower values of parameter i_0 (Fig. 13, bottom), the case with high rainfall intensity and low filling rate (Case 3) is the one that shows the highest number of occurrences of high differences in runoff production between models. In this case, we have a higher frequency of time steps of the rainfall-runoff transformation benefitting from the GRSDi model structure. The changes in occurrences highlight the fact that the modification introduced in the original semi-distributed GRSD model added a degree of versatility to the model when simulating runoff production over different modelling units and outlets of the catchment and a long time period.

4 Discussion and conclusions

This study investigated the potential of a simple modification introduced in a conceptual, hourly, semi-distributed hydrological model (GRSD model) to improve the simulation of extreme flood events generated by intense rainfalls in a flash-flood-prone catchment in the Mediterranean region in southwest France. The semi-distributed hydrological model GRSD was modified to better simulate flash floods occurring after long dry periods, while also simulating well other floods occurring during or after wet periods in a typical Mediterranean catchment. The model adaptation consisted in introducing a dependency on the rainfall intensity in the production rate, which is calculated before the rainfall "flows" into the model's production store. The runoff production is then modified and can be increased when intense rain falls over dry soils (which, in the model, is represented by a production store with a low level at the time the rain falls in the catchment). The modification introduced one additional free parameter to calibrate. This parameter varies within the interval [0; 100] [mm h^{-1}] and modifies the behaviour of the production rate: the closer its value is to 100 [mm h^{-1}], the more the adapted structure behaves like the original model structure in terms of net rainfall. The performance of the modified model structure was evaluated over a 10-year period of hourly flow observations and simulations at 31 gauged sub-catchments and for four selected flood events. The analysis investigated model versatility considering also 109 ungauged modelling units within the catchment.

The long-term assessment of model performance, based on the KGE criterion, showed that for most of the outlets, the model adaptation does not deteriorate model simulations when compared to the original GRSD model simulations. Where the performance of the GRSDi model is lower, the differences in KGE values are less than 0.1. The event-based assessment showed that the most important improvement brought by the GRSDi model was observed in the simulation of the magnitude of the flood peaks. It compensated for the underestimations of the original GRSD model during the flood events occurring in autumn, resulting from intense rains falling after a long and dry summer period. The difficulties of the GRSD model in simulating floods in the beginning of the hydrological year (autumn events) can be explained by the behaviour of its production (soil moisture accounting) store. In the Mediterranean regime, average precipitation is low in summer and temperatures are high. In the GRSD model, most of the available water from the production store evaporates and its level is often low by the end of summer. If we use GRSD's original equation to obtain the production rate with a low production store level, the amount of water flowing to the rest of the model will not be sufficient to simulate the flood peaks correctly; most of the water entering the model will be used to fill the production store. This behaviour will persist despite the high values of hourly rain falling over the catchment. The typical short durations of the events are not enough to fill the production store and produce high amounts of net rainfall. The adapted model (GRSDi) performs better for these specific flood events, which occur during short time periods and limited areas but present major issues, as these are events that may cause damages and sometimes human losses when not well forecast by hydrological models. We note that while the analysis focused on peak discharge and time of peak, which are relevant for threshold-based flood alerts, mismatches in terms of flood volume could also be interesting to assess for other operational purposes of hydrological models.

One of the advantages of the model adaptation proposed here is that it supports model versatility, as it favours the use of a single model to simulate different conditions of flow intensity and flood event antecedent conditions. Model versatility was investigated by quantifying the differences in runoff production between the two models over the modelling units of the semi-distributed modelling framework and along the hourly time steps of the 10-year study period. In the majority of simulation time steps, no differences in runoff production were found between the simulations using the GRSDi and the GRSD models, which was expected as high flows and floods are rare occurrences. The versatility of the adaptation proposed was clearly shown for the simulation time steps where low, medium and high differences were observed. These were time steps when rainfall intensities were located in the upper tail of the non-zero hourly rainfall distribution. Specifically for the high differences in runoff, they were more frequently observed for specific periods of the year when observed rainfall values were high and the levels of the model production store were low. This behaviour was particularly accentuated in modelling units with low values of the additional parameter of the GRSDi model. The results indicate that the modification introduced in the original GRSD model structure is activated when the model needs to adapt to specific conditions, illustrating the added value of the versatility provided by the modified

structure, despite its simplicity. More complex model adaptations (e.g. adding upper layers for overland flow in the production store) might further improve model performance – but probably at the cost of introducing additional parameters to be calibrated and increasing computational time.

The proposed model adaptation integrates a runoff generation process in the original GRSD model structure by adding a free parameter (i_0). It could be interesting to explore the links between this parameter and soil characteristics (or hydraulic conductivity). Additionally, we observed that in some cases the calibration of this parameter led to reaching its upper bound. Further research could explore this upper bound and analyse how it may affect model behaviour or increase its versatility, e.g. for flood modelling in urban catchments. Although the modification proposed is linked to the way the original model is structured, its conceptualization and its equations, it could be adapted to other types of models, particularly storage-based models where representing the runoff generation process targeted in this paper is needed. The rationale remains the same: instead of changing the whole model (which is not often possible in operational settings), one can adapt the structure of an existing model to target low performance during specific flood situations. The potential of using a versatile model in the context of real-time flood forecasting is another interesting perspective of this study. Forecasting systems usually run within operational setups that rarely allow changing the structure of the hydrological model during the forecasting of a flood event. An adaptive model in real-time flood forecasting can be particularly useful in the case of flash floods, since these are the result of localized intense rainfall that can generate different hydrological responses depending on the rainfall intensities and the catchment's initial conditions. These events require short model run times for effective flood alert and response. The use of several model structures, especially in the operational context, may not be feasible, and having a calibrated model running continuously without the need for a specific parameter set for each type of forecast flood event can be an asset.

Acknowledgements

Disclosure statement

ORCID

Daniela Peredo ⬦ http://orcid.org/0000-0001-5769-825X
Maria-Helena Ramos ⬦ http://orcid.org/0000-0003-1133-4164
Vazken Andréassian ⬦ http://orcid.org/0000-0001-7124-9303
Ludovic Oudin ⬦ http://orcid.org/0000-0002-3712-0933

References

Addor, N. and Melsen, L.A., 2019. Legacy, rather than adequacy, drives the selection of hydrological models. *Water Resources Research*, 55, 378–390. doi:10.1029/2018WR022958

Alaoui, A., *et al.*, 2018. Does soil compaction increase floods? A review. *Journal of Hydrology*, 557, 631–642. doi:10.1016/j.jhydrol.2017.12.052

Anquetin, S., *et al.*, 2010. Sensitivity of the hydrological response to the variability of rainfall fields and soils for the Gard 2002 flash-flood event. *Journal of Hydrology*, 394, 134–147. doi:10.1016/j.jhydrol.2010.07.002

Bentura, P.L.F. and Michel, C., 1997. Flood routing in a wide channel with a quadratic lag-and-route method. *Hydrological Sciences Journal*, 42, 169–189. doi:10.1080/02626669709492018

Berghuijs, W.R., *et al.*, 2019. The relative importance of different flood-generating mechanisms across Europe. *Water Resources Research*, 55, 4582–4593. doi:10.1029/2019WR024841

Beven, K., 1997. TOPMODEL: a critique. *Hydrological Processes*, 11, 17. doi:10.1002/(SICI)1099-1085(199707)11:9<1069::AID-HYP545>3.0.CO;2-O

Beven, K. and Freer, J., 2001. A dynamic TOPMODEL. *Hydrological Processes*, 15, 1993–2011. doi:10.1002/hyp.252

Beven, K.J. and Kirkby, M.J., 1979. A physically based, variable contributing area model of basin hydrology. *Hydrological Sciences Bulletin*, 24, 43–69. doi:10.1080/02626667909491834

Borga, M., *et al.*, 2007. Hydrometeorological analysis of the 29 August 2003 flash flood in the Eastern Italian Alps. *Journal of Hydrometeorology*, 8, 1049–1067. doi:10.1175/JHM593.1

Champeaux, J.L., *et al.*, 2009. Les mesures de précipitations et l'estimation des lames d'eau à Météo-France: état de l'art et perspectives. *La Houille Blanche*, 5, 28–34. doi:10.1051/lhb/2009052

Ciarapica, L. and Todini, E., 2002. TOPKAPI: a model for the representation of the rainfall-runoff process at different scales. *Hydrological Processes*, 16, 207–229. doi:10.1002/hyp.342

Clark, M.P., *et al.*, 2015. A unified approach for process-based hydrologic modeling: 1. *Modeling Concept. Water Resources Research*, 51 (4), 2498-2514. doi:10.1002/2015WR017198

Clark, M.P., Kavetski, D., and Fenicia, F., 2011. Pursuing the method of multiple working hypotheses for hydrological modeling. *Water Resources Research*, 47 (9). doi:10.1029/2010WR009827

Coron, L., *et al.*, 2017. The suite of lumped GR hydrological models in an R package. *Environmental Modelling & Software*, 94, 166–171. doi:10.1016/j.envsoft.2017.05.002

de Lavenne, A., *et al.*, 2016. Spatial variability of the parameters of a semi-distributed hydrological model. *Proceedings of the International Association of Hydrological Sciences*, 373, 87–94. doi:10.5194/piahs-373-87-2016

de Lavenne, A., *et al.*, 2019. A regularization approach to improve the sequential calibration of a semidistributed hydrological model. *Water Resources Research*, 55, 8821–8839. doi:10.1029/2018WR024266

Delrieu, G., *et al.*, 2005. The catastrophic flash-flood event of 8–9 September 2002 in the Gard region, France: a first case study for the Cévennes–Vivarais Mediterranean hydrometeorological observatory. *Journal of Hydrometeorology*, 6, 34–52. doi:10.1175/JHM-400.1

Douinot, A., *et al.*, 2018. Using a multi-hypothesis framework to improve the understanding of flow dynamics during flash floods. *Hydrology and Earth System Sciences*, 22, 5317–5340. doi:10.5194/hess-22-5317-2018

Dunne, T. and Black, R.D., 1970. Partial area contributions to storm runoff in a small New England watershed. *Water Resources Research*, 6, 1296–1311. doi:10.1029/WR006i005p01296

Edijatno, N. and Michel, C., 1989. Un modèle pluie-débit journalier à trois paramètres [A three-parameter daily rainfall-runoff model]. *La Houille Blanche*, 2, 113–121. doi:10.1051/lhb/1989007

Faccini, F., et al., 2016. The Bisagno stream catchment (Genoa, Italy) and its major floods: geomorphic and land use variations in thelast three centuries. Geomorphology, 273, 14–27. doi:10.1016/j.geomorph.2016.07.037

Fenicia, F., et al., 2014. Catchment properties, function, and conceptual model representation : is there a correspondence? Hydrological Processes, 28 (4), 2451-2467. doi:10.1002/hyp.9726

Fenicia, F., Kavetski, D., and Savenije, H.H.G., 2011. Elements of a flexible approach for conceptual hydrological modeling: 1. Motivation and theoretical development. Water Resources Research, 47 (11). doi:10.1029/2010WR010174

Ferré, T.P.A. and Warrick, A.W., 2005. Infiltration. In: D. Hillel, ed. Encyclopedia of soils in the environment. Oxford: Elservier, 254–260.

Ficchì, A., Perrin, C., and Andréassian, V., 2016. Impact of temporal resolution of inputs on hydrological model performance: an analysis based on 2400 flood events. Journal of Hydrology, 538, 454–470. doi:10.1016/j.jhydrol.2016.04.016

Ficchì, A., Perrin, C., and Et Andréassian, V., 2019. Hydrological modelling at multiple sub-daily time steps: model improvement via flux-matching. Journal of Hydrology, 575, 1308–1327. doi:10.1016/j.jhydrol.2019.05.084

Garambois, P., et al., 2014. Analysis of flash flood triggering rainfall for a process-oriented hydrological model. Atmospheric Research, 137, 14–24. doi:10.1016/j.atmosres.2013.09.016

Garavaglia, F., et al., 2017. Impact of model structure on flow simulation and hydrological realism: from a lumped to a semi-distributed approach. Hydrology and Earth System Sciences, 21, 3937–3952. doi:10.5194/hess-21-3937-2017

Gaume, E., et al., 2004. Hydrological analysis of the river Aude, France, flash flood on 12 and 13 November 1999. Journal of Hydrology, 286, 135–154. doi:10.1016/j.jhydrol.2003.09.015

Gaume, E., et al., 2016. Mediterranean extreme floods and flash floods. In: The Mediterranean region under climate change. A scientific update. Marseille, France: IRD Éditions, 133–144.

Gourley, J.J., et al., 2017. The FLASH project: improving the tools for flash flood monitoring and prediction across the United States. Bulletin of the American Meteorological Society, 98, 361–372. doi:10.1175/BAMS-D-15-00247.1

Gupta, H.V., et al., 2009. Decomposition of the mean squared error and NSE performance criteria: implications for improving hydrological modelling. Journal of Hydrology, 377, 80–91. doi:10.1016/j.jhydrol.2009.08.003

Habets, F., et al., 2008. The SAFRAN-ISBA-MODCOU hydrometeorological model applied over France. Journal of Geophysical Research, 113, D06113. doi:10.1029/2007JD008548

Hamman, J.J., et al., 2018. The Variable Infiltration Capacity model version 5 (VIC-5): infrastructure improvements for new applications and reproducibility. Geoscientific Model Development, 11, 3481–3496. doi:10.5194/gmd-11-3481-2018

Horton, R.E., 1945. Erosional development of streams and their drainage basins; hydrophysical approach to quantitative morphology. Geological Society of America Bulletin, 56, 275–370. doi:10.1130/0016-7606(1945)56[275:EDOSAT]2.0.CO;2

Laurantin, O., 2008. Antilope: hourly rainfall analysis merging radar and rain gauge data. In: Proceedings of the international symposium on weather radar and hydrology, 10–12 March 2008 Grenoble, 2–8.

Le Lay, M. and Saulnier, G.M., 2007. Exploring the signature of climate and landscape spatial variabilities in flash flood events: case of the 8–9 September 2002 Cévennes-Vivarais catastrophic event. Geophysical Research Letters, 34, L13401. doi:10.1029/2007GL029746

Le Moine, N., Andréassian, V., and Mathevet, T., 2008. Confronting surface- and groundwater balances on the La Rochefoucauld-Touvre karstic system (Charente, France): closing the catchment-scale water balance - a case study. Water Resources Research, 44, W03403. doi:10.1029/2007WR005984

Leleu, I., et al., 2014. La refonte du système d'information national pour la gestion et la mise à disposition des données hydrométriques. La Houille Blanche, 1, 25–32. doi:10.1051/lhb/2014004

Liang, X., Wood, E., and Burges, S., 1994. A simple hydrologically based model of land surface water and enery fluxes for general circulation models. Journal of Geophysical Research, 99, 14415–14428. doi:10.1029/94JD00483

Liu, Z. and Todini, E., 2002. Towards a comprehensive physically-based rainfall-runoff model. Hydrology and Earth System Sciences, 6 (5), 859–881. doi:10.5194/hess-6-859-2002

Llasat, M.C., et al., 2016. Trends in flash flood events versus convective precipitation in the Mediterranean region: the case of Catalonia. Journal of Hydrology, 541, 24–37. doi:10.1016/j.jhydrol.2016.05.040

Lobligeois, F., et al., 2014. When does higher spatial resolution rainfall information improve streamflow simulation? An evaluation using 3620 flood events. Hydrology and Earth System Sciences, 18 (2), 575-594. doi:10.5194/hess-18-575-2014

Melsen, L.A., et al., 2016. HESS opinions: the need for process-based evaluation of large-domain hyper-resolution models. Hydrology and Earth System Sciences, 20 (3), 1069-1079. doi:10.5194/hess-20-1069-2016

Nguyen, S. and Bouvier, C., 2019. Flood modelling using the distributed event-based SCS-LR model in the Mediterranean Real Collobrier catchment. Hydrological Sciences Journal, 64 (11), 1351–1369. doi:10.1080/02626667.2019.1639715

Obled, C., Zin, I., and Hingray, B., 2009. Choix des pas de temps et d'espace pour des modélisations parcimonieuses en hydrologie des crues. La Houille Blanche, 5, 81–87. doi:10.1051/lhb/2009059

Oudin, L., et al., 2005. Which potential evapotranspiration input for a rainfall-runoff model? Part 2 – towards a simple and efficient PE model for rainfall-runoff modelling. Journal of Hydrology, 303 (1–4), 290–306. doi:10.1016/j.jhydrol.2004.08.026

Pagano, T.C., et al., 2014. Challenges of operational river forecasting. Journal of Hydrometeorology, 15, 1692–1707. doi:10.1175/JHM-D-13-0188.1

Perrin, C., Michel, C., and Andréassian, V., 2001. Does a large number of parameters enhance model performance? Comparative assessment of common catchment model structures on 429 catchments. Journal of Hydrology, 242 (3–4), 275–301. doi:10.1016/S0022-1694(00)00393-0

Perrin, C., Michel, C., and Andréassian, V., 2003. Improvement of a parsimonious model for streamflow simulation. Journal of Hydrology, 279, 275–289. doi:10.1016/S0022-1694(03)00225-7

Reed, S., et al., 2004. Overall distributed model intercomparison project results. Journal of Hydrology, 298, 27–60. doi:10.1016/j.jhydrol.2004.03.031

Roux, H., et al., 2011. A physically-based parsimonious hydrological model for flash floods in Mediterranean catchments. Natural Hazards and Earth System Science, 11, 2567–2582. doi:10.5194/nhess-11-2567-2011

Seiller, G., Anctil, F., and Perrin, C., 2012. Multimodel evaluation of twenty lumped hydrological models under contrasted climate conditions. Hydrology and Earth System Sciences, 16, 1171–1189. doi:10.5194/hess-16-1171-2012

Sivapalan, M., Beven, K., and Wood, E.F., 1987. On hydrologic similarity: 2. A scaled model of storm runoff production. Water Resources Research, 23, 2266–2278. doi:10.1029/WR023i012p02266

Smith, M.B., et al., 2012. Results of the DMIP 2 Oklahoma experiments. Journal of Hydrology, 418–419, 17–48. doi:10.1016/j.jhydrol.2011.08.056

Stein, L., Pianosi, F., and Woods, R., 2020. Event based classification for global study of river flood generating processes. Hydrological Processes, 34, 1514–1529. doi:10.1002/hyp.13678

van Esse, W.R., et al., 2013. The influence of conceptual model structure on model performance : a comparative study for 237 French catchments. Hydrology and Earth System Sciences, 17 (10), 4227-4239. doi:10.5194/hess-17-4227-2013

Velázquez, J.A., et al., 2011. Can a multi-model approach improve hydrological ensemble forecasting? A study on 29 French catchments using 16 hydrological model structures. Advances in Geosciences, 29, 33-42. doi:10.5194/adgeo-29-33-2011

Vidal, J.-P., *et al.*, 2010. A 50-year high-resolution atmospheric reanalysis over France with the Safran system. *International Journal of Climatology*, 30, 1627–1644. doi:10.1002/joc.2003

Viglione, A., *et al.*, 2010. Generalised synthesis of space–time variability in flood response: an analytical framework. *Journal of Hydrology*, 394, 198–212. doi:10.1016/j.jhydrol.2010.05.047

Viglione, A. and Rogger, M., 2015. Chapter 1 - flood processes and hazards. *In*: J.F. Shroder, P. Paron, and G.D. Baldassarre, eds. *Hydrometeorological hazards, risks and disasters*. Boston: Elsevier, 3–33. doi:10.1016/B978-0-12-394846-5.00001-1

Vincendon, B., *et al.*, 2010. Benefit of coupling the ISBA land surface model with a TOPMODEL hydrological model version dedicated to Mediterranean flash-floods. *Journal of Hydrology*, 394, 256–266. doi:10.1016/j.jhydrol.2010.04.012

Vivoni, E.R., *et al.*, 2007. Controls on runoff generation and scale-dependence in a distributed hydrologic model. *Hydrology and Earth System Sciences*, 11, 1683–1701. doi:10.5194/hess-11-1683-2007

Wagener, T., *et al.*, 2001. A framework for development and application of hydrological models. *Hydrology and Earth System Sciences*, 5 (1), 13-26. doi:10.5194/hess-5-13-2001